

NASA TECHNICAL NOTE



NASA TN D-5489

c. 1

NASA TN D-5489



LOAN COPY: RETURN TO  
AFWL (WL0L-2)  
KIRTLAND AFB, N MEX

## CALCULATION OF THERMAL-FATIGUE LIFE BASED ON ACCUMULATED CREEP DAMAGE

*by David A. Spera*

*Lewis Research Center*

*Cleveland, Ohio*



0132146

1. Report No. NASA TN D-5489		2. Government Accession No.		3. Recipient's Catalog No.	
4. Title and Subtitle CALCULATION OF THERMAL-FATIGUE LIFE BASED ON ACCUMULATED CREEP DAMAGE		5. Report Date October 1969		6. Performing Organization Code	
		8. Performing Organization Report No. E-4950		10. Work Unit No. 129-03	
7. Author(s) David A. Spera		9. Performing Organization Name and Address Lewis Research Center National Aeronautics and Space Administration Cleveland, Ohio, 44135		11. Contract or Grant No.	
12. Sponsoring Agency Name and Address National Aeronautics and Space Administration Washington, D. C. 20546		13. Type of Report and Period Covered Technical Note		14. Sponsoring Agency Code	
		15. Supplementary Notes			
16. Abstract A method is presented for predicting the onset of thermal-fatigue cracking in high-temperature components under service conditions. Starting from basic material properties, life is calculated by considering two distinct failure modes: (1) cyclic creep-rupture, using a modification of the well-known life-fraction rule proposed by Robinson and Taira, and (2) conventional, time-independent, low-cycle fatigue, using empirical equations of the Method of Universal Slopes developed by Manson. The method is illustrated by using Glenny-type thermal-fatigue test data on the nickel-base alloy Nimonic 90. In 24 of the 28 cases analyzed, cyclic creep-rupture was the dominant failure mode.					
17. Key Words (Suggested by Author(s)) Thermal fatigue Creep Life calculation			18. Distribution Statement Unclassified - unlimited		
19. Security Classif. (of this report) Unclassified	20. Security Classif. (of this page) Unclassified	21. No. of Pages 38	22. Price* \$3.00		

\*For sale by the Clearinghouse for Federal Scientific and Technical Information  
Springfield, Virginia 22151

# CALCULATION OF THERMAL-FATIGUE LIFE BASED ON ACCUMULATED CREEP DAMAGE

by David A. Spera

Lewis Research Center

## SUMMARY

A method is presented for predicting the onset of thermal-fatigue cracking in high-temperature components such as turbine blades and disks which are subjected to arbitrary, complex cycles of temperature and load. It is proposed that thermal-fatigue life can be determined solely from the basic mechanical properties of a material by calculating lives for each of two distinct and independent failure modes: (1) cyclic creep-rupture, using a modification of the well-known life-fraction rule proposed by Robinson and Taira, and (2) conventional low-cycle fatigue, using the empirical equations of the Method of Universal Slopes developed by Manson. Equations are presented in sufficient detail to completely define the analytical procedure.

The proposed method of life analysis is illustrated and evaluated by using data from Glenny-type thermal-fatigue tests, as reported in the literature. In these tests, tapered-disk specimens of the nickel alloy Nimonic 90 were heated and cooled in beds of fluidized sand to produce cracks similar to those found on the leading and trailing edges of turbine blades and vanes after service. In this study, temperatures, strains, stresses, and finally lives are calculated for the disk specimens, which were cycled under a variety of temperature and time conditions, with and without internal air-cooling. It is found in 24 of the 28 cases analyzed that cyclic creep-rupture is the dominant failure mode. Calculated and observed lives generally are in good agreement. This investigation indicates that efforts to predict and eventually improve the thermal-fatigue resistance of a high-temperature alloy or component should be focused on the calculation and reduction of creep damage.

## INTRODUCTION

This investigation was conducted to develop a method for predicting the onset of thermal-fatigue cracking in a high-temperature component such as a turbine blade or

disk. Thermal fatigue is defined as the cracking of a material primarily by repeated heating and cooling which induces cyclic internal thermal stresses. In addition, stresses caused by external mechanical loads may also contribute to thermal-fatigue failure. Each thermal-fatigue cycle is a complex combination of changing stresses, strains, temperatures, and material properties. Stress, temperature, and time conditions may be sufficient to cause both instantaneous plastic strain and time-dependent creep strain during each cycle. Therefore, a general method for calculating thermal-fatigue life must apply to a cycle in which various types of material behavior are present in arbitrary combinations. This study presents a method of life calculation which can be used to predict the start of thermal-fatigue cracking caused by a general thermomechanical cycle.

A review of the research which forms a background for this investigation has been given in reference 1. Some 30 references were discussed to trace the development of fatigue theory during the last 110 years. In general, the thermal-fatigue theory proposed in references 1 to 3 and further developed herein differs from previous work in one or more of the following ways:

(1) Thermal fatigue is considered to be primarily a creep-rupture phenomenon rather than a modification of conventional room-temperature fatigue.

(2) Creep-rupture is assumed to be a possible failure mechanism in any cycle, rather than being limited to cycles which contain tensile mean stress.

(3) The proposed theory applies directly to the complete service cycle of load and temperature, rather than being limited to a specific idealized laboratory test such as isothermal strain-cycling.

(4) Modifications are presented to existing cumulative damage rules for creep-rupture under nonsteady conditions to account for the potentially beneficial effect of eliminating net creep strain.

(5) The proposed theory predicts in quantitative terms the effect on thermal-fatigue life of various cycle parameters such as maximum and minimum temperatures, rates of heating and cooling, and hold periods.

In many ways this investigation is a continuation of pioneering work performed by P. W. H. Howe at the National Gas Turbine Establishment (England). In 1962, Howe published what can rightly be termed the first complete thermal-fatigue analysis (ref. 4). The term "complete" stems from the fact that all stages of the general thermal-fatigue problem were treated: (1) determining transient temperature distributions, (2) estimating the stresses using creep data, and (3) obtaining thermal-fatigue life by using isothermal mechanical endurance data for slowly repeated cycles of tension. It was emphasized that the important factor in determining life was time-dependence of the same type as expressed in creep data, rather than a time-independent effect such as plastic deformation. Following this hypothesis, the present investigation will relate thermal-fatigue life directly to conventional creep life, without recourse to the cyclic mechanical tests used by Howe.

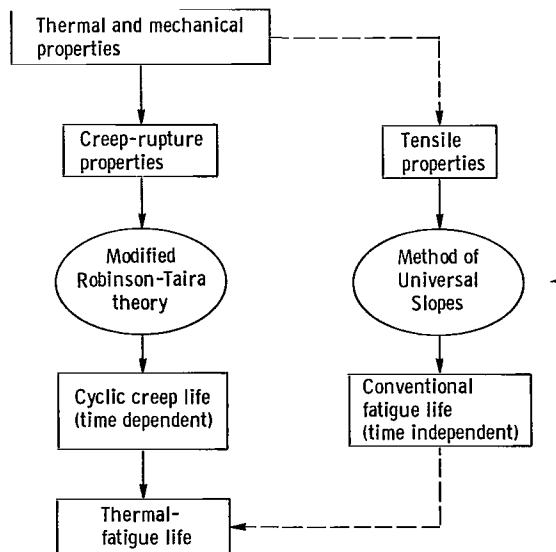


Figure 1. - Proposed thermal-fatigue theory.

The method of analysis which will be used in this investigation is illustrated in figure 1. It is postulated that the thermal-fatigue life resulting from any thermal-mechanical cycle can be determined solely from the conventional mechanical and thermal properties of a material by calculating lives for each of two distinct and independent failure modes: (1) cyclic creep-rupture, and (2) conventional low-cycle fatigue. As implied in figure 1, cyclic creep-rupture is the most common failure mode, particularly in the short and intermediate life ranges. Life in this mode is calculated from conventional creep rates and rupture times by a modification of the linear cumulative damage rule proposed by Robinson (ref. 5) and Taira (ref. 6). The modified Robinson-Taira theory unifies two apparently different phenomena - cyclic thermal fatigue and static creep-rupture - without the use of empirical constants derived from cyclic tests.

Conventional low-cycle fatigue is considered to be an alternate failure mode which may be dominant for longer thermal-fatigue lives. Low-cycle fatigue life is calculated from conventional short-time tensile properties by the existing Method of Universal Slopes developed by Manson (ref. 7). This method relates cyclic life to the mechanical strain range experienced by the material and is independent of time parameters such as frequency. In its original form, the Method of Universal Slopes applies only to fatigue in the absence of any creep effects. However, simple modifications have been proposed in the literature to extend its range of application to include high-temperature fatigue. These modifications are discussed herein and are particularly appropriate for those cases in which it is impractical to make a complete stress analysis.

This study is presented in the following manner: First, equations are given in sufficient detail to completely define the proposed analytical method. Secondly, these equa-

tions are used to calculate thermal-fatigue lives for comparison with Glenny-type thermal-fatigue data for the nickel-base alloy Nimonic 90. Thirdly, the calculated and observed lives are used as a basis for drawing general conclusions about the phenomenon of thermal fatigue and the usefulness of the proposed life analysis method.

In summary, this investigation uses the hypothesis that the process of crack initiation during thermal fatigue of a turbine blade is often the same as the process of rupture during conventional monotonic creep. This leads to a proposed method of life analysis which is evaluated by using the results of thermal-fatigue tests obtained from the literature.

## GLENNY-TYPE THERMAL-FATIGUE TESTING

Glenny-type thermal-fatigue testing refers to the use of tapered-disk specimens which are alternately heated and cooled rapidly in beds of fluidized solids (ref. 8). A diagram of the fluidized-bed facility developed by Glenny and his associates is shown in figure 2. In this facility, the beds are used in pairs, one each for heating and cooling. Compressed air enters diffusion chambers below each bed and passes upward through perforated plates which support the actual beds. The beds are filled with ceramic particles such as zircon sand. As the air passes upward through the particles they become levitated or "fluidized" under the action of drag forces and develop a churning action analogous to that of a rapidly boiling liquid. Heating is accomplished by electric-resistance elements immersed directly in one bed, while cooling is achieved in the other bed by a water jacket. The large heat capacity of the beds and the churning action of the

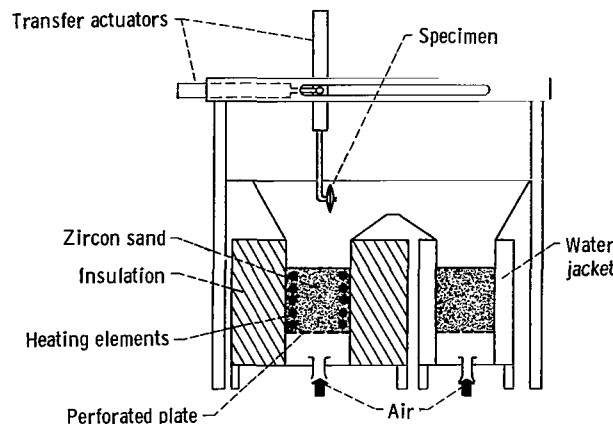
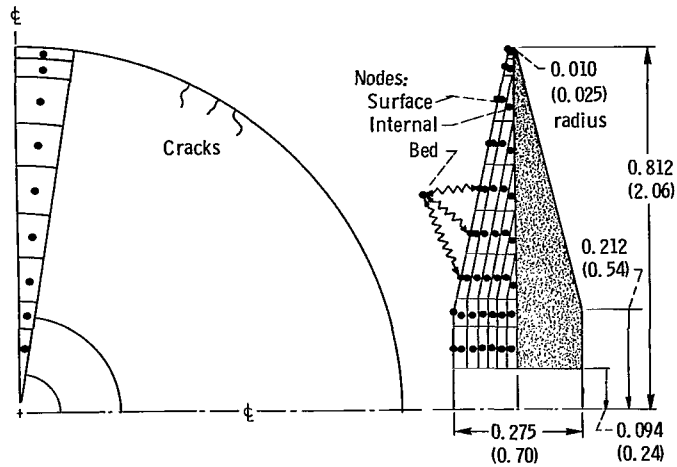
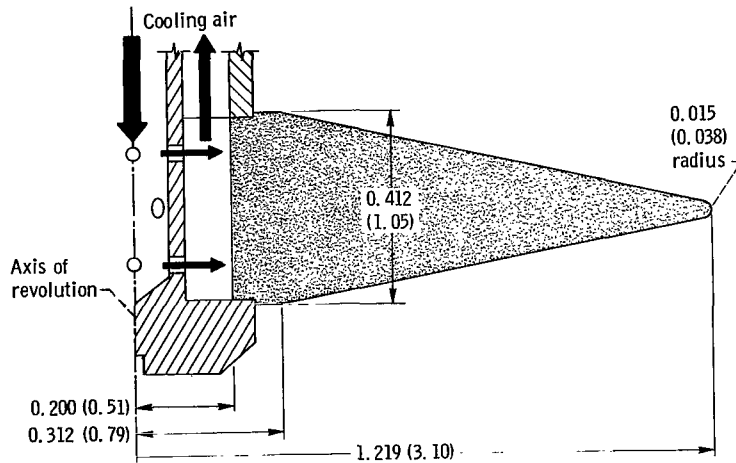


Figure 2. - Diagram of fluidized-bed thermal-fatigue facility developed by Glenny, et al. (refs. 8 and 12).



(a) Standard tapered disk (ref. 8).



(b) Core-cooled tapered disk (ref. 12).

Figure 3. - Thermal-fatigue specimens. Dimensions are in inches (cm).

particles are conducive to rapid heating and cooling. Also, the high thermal inertia of the beds permits accurate temperature control over an extended period of time.

Glenny-type thermal-fatigue tests were first conducted using a "standard" tapered-disk specimen such as the one depicted in figure 3(a). During rapid heating and cooling, the thin periphery of the disk experiences faster temperature changes than the bulkier core section. The core constrains the free thermal expansion and contraction of the periphery, inducing cyclic thermal stresses which eventually cause radial cracks to appear at the thin edge, as shown in figure 3(a). Thus, failure in a tapered disk occurs under conditions of (1) rapid temperature range with respect to both time and distance, (2) indeterminate uniaxial stress, and (3) high ratio of surface to volume. These conditions are also typical of the leading and trailing edges of turbine blades and vanes. The stand-

ard disk was used extensively by Glenny et al. (refs. 8 to 10) and also by Franklin, Heslop, and Smith (ref. 11) for their comparative study of thermal fatigue in 24 different high-temperature alloys.

The central or "core" portions of some turbine blades are cooled by air flowing through spanwise passages. This airflow causes a decrease in average section temperature and a corresponding increase in creep-rupture strength with which to resist centrifugal loads. J. T. Roberts (ref. 12) conducted tests in a fluidized-bed facility to see if core-cooling would also increase thermal-fatigue life. Figure 3(b) shows how the standard tapered-disk specimen was modified to provide for core-cooling in these tests.

The general size of Glenny's standard disk was increased by 50 percent, while the central hole was further enlarged to receive a hollow support shaft with two concentric passages. Air at 100<sup>o</sup> F (310 K) and 0.018 pound per second (8.2 g/sec) was conducted to the specimen through the inner passage, separated into 12 jets by radial holes in the shaft, impinged on the periphery of the central hole in the disk, and then exhausted through the outer passage in the support shaft.

## METHOD OF ANALYSIS

The following description of the analytical method contains some details which pertain specifically to the Glenny-type thermal-fatigue tests described in the previous section. However, the general method is applicable to any high-temperature component such as a turbine blade, vane, or disk. The complete analytical procedure consists of five steps:

- Step 1: Calculation of transient temperatures throughout the specimen, using measured transient temperatures from references 12 and 13 to determine surface heat-transfer coefficients between the specimen and the fluidized beds
- Step 2: Calculation of transient strains at the periphery of the disk using the results of step 1 and equations from reference 14
- Step 3: Calculation of the elastic, plastic, and creep components of peripheral strain using the results of steps 1 and 2, thereby obtaining the transient peripheral stresses
- Step 4: Calculation of the creep damage per cycle using the results of step 3, the monotonic creep-rupture strength of the alloy, and a linear cumulative damage theory, thereby obtaining the number of cycles to failure in the creep mode
- Step 5: Calculation of the number of cycles to failure in conventional low-cycle fatigue, using the range of strain calculated in step 2, the short-time tensile properties of the alloy, and an empirical fatigue equation

The temperature, stress, and strain conditions at the peripheral surface of the disk are

used to calculate creep and fatigue damage. Therefore, the term "calculated life" is defined herein as the theoretical number of cycles required to cause failure of the surface. This will be compared with the observed number of cycles required to initiate cracking of the periphery of the specimen.

## Step 1: Calculation of Temperatures

In a thermal-fatigue specimen or an engine component, two types of temperature data are usually required: (1) the general distribution of temperature throughout the part, with which to calculate total strains during the cycle and (2) the temperature at the probable points of failure in the part, with which to calculate local thermal expansion and material properties. A method for calculating these temperatures is generally required because temperature measurements can normally be obtained only at a small number of points in the part and often not directly at the probable points of failure. For these reasons, a great deal of effort has been given to the development of heat-transfer theory and practice which can be used to expand limited temperature measurements into complete temperature distributions.

In this investigation, an existing computer code called TOSSA (acronym for Transient or Steady-State Analysis) was used to calculate temperatures. The heat-transfer analysis was started by constructing the nodal diagram shown in figure 3(a). This diagram converts the disk specimen into a lumped-parameter system in which all heat is stored at the node points (shown as black dots) or is conducted between nodes along connectors which may be internal, surface, or bed connectors. The rate at which heat is transferred along connectors or stored at nodes is determined by (1) the surface heat-transfer coefficients, (2) thermal conductivity, (3) specific heat, (4) density, and (5) the dimensions of the nodes and connectors. Quantities (1) and (2) were adjusted until the calculated peripheral and volume average temperatures agreed with measured values as reported in reference 13. Details of the transient temperature analysis are given in reference 3.

## Step 2: Calculation of Strains

The calculation of peripheral elastic strains was carried on simultaneously with the calculation of transient temperatures (step 1) by adding a new subroutine to the existing TOSSA code. Equations for this subroutine were taken from reference 14 and are repeated in reference 3. The disk is assumed to be composed of a series of concentric cylindrical layers of variable length which are assumed to remain cylindrical during heating

and cooling. Each cylindrical layer is assumed to be uniformly at its average temperature, stress, and strain states. It is assumed that the disk specimens are thin enough to make this one-dimensional analysis acceptable. However, this investigation indicates that a more complex two-dimensional analysis would be justified to determine the effect of axial temperature gradients on the calculated peripheral strains.

The calculation of the elastic, plastic, and creep components of strain is based on the assumption that the calculated total strains are approximately the same for a given temperature distribution whether or not plastic strain is assumed to occur. Thus, for a uniaxial state of stress such as that which exists at the disk periphery,

$$\epsilon_t \equiv \epsilon_m + \epsilon_T \approx \epsilon_o \quad (1a)$$

in which

$\epsilon$  peripheral strain, percent

t, m, T total, mechanical, and thermal, respectively

$\epsilon_o$  calculated total strain, assuming completely elastic behavior, percent

Also,

$$\left. \begin{aligned} \epsilon_m &\equiv \epsilon_e + \epsilon_p + \epsilon_c \\ \epsilon_T &= \bar{\alpha}(T - RT) \end{aligned} \right\} \quad (1b)$$

in which

e, p, c elastic, plastic, and creep, respectively

$\bar{\alpha}$  mean coefficient of thermal expansion, percent/<sup>o</sup>F (percent/K)

T temperature, <sup>o</sup>F (K)

RT room temperature, 70<sup>o</sup> F (290 K)

Equation (1a) defines the "method of strain invariance" which was proposed by Mendelson and Manson (ref. 15) on the basis of their analysis of several kinds of thermoelastoplastic problems. Relative constancy of total strain with and without plastic flow indicates that, for thermal loads, strains depend almost completely on compatibility conditions which are geometric relations independent of the actual stress-strain behavior.

### Step 3: Calculation of Stresses

Equations (1) may be combined to give

$$\epsilon_e = \epsilon_o - \epsilon_p - \epsilon_c - \bar{\alpha}(T - RT)$$

or

$$S = E [\epsilon_o - \epsilon_p - \epsilon_c - \bar{\alpha}(T - RT)] \quad (2a)$$

in which

S peripheral stress, ksi (kN/cm<sup>2</sup>)

E Young's Modulus, ksi/percent (kN/cm<sup>2</sup>/percent)

The amount of instantaneous plastic strain  $\epsilon_p$  is calculated by assuming ideally plastic behavior at known minimum and maximum stress limits, so that

$$S_{\min} \leq S \leq S_{\max} \quad (2b)$$

The minimum and maximum stresses are reached during the heating and cooling half-cycles, respectively. Therefore, combining equations (2a) and (2b) gives

$$\epsilon_{p,i} = \begin{cases} \epsilon_{p,i-1} & S_{\min} < S_i < S_{\max} \\ \text{or} \\ \epsilon_{o,i} - \frac{S_{\min}}{E_i} - \epsilon_{c,i} - \epsilon_{T,i} & S_i = S_{\min} \\ \text{or} \\ \epsilon_{o,i} - \frac{S_{\max}}{E_i} - \epsilon_{c,i} - \epsilon_{T,i} & S_i = S_{\max} \end{cases} \quad (3)$$

in which  $i$  is the time-increment index. The minimum and maximum stresses are actually the yield strength of the alloy at the temperatures which coincide with the minimum and maximum mechanical strains. Their exact values cannot be determined accurately in advance because of the possibility that cyclic strain-hardening or strain-softening will

raise or lower the yield strength, respectively. Fortunately, the calculated thermal-fatigue life is not sensitive to moderate variations in yield strength, so the conventional tensile-test values of yield strength are usually satisfactory.

The creep strain at time  $i$  may be expressed as

$$\epsilon_{c,i} = \epsilon_{c,i-1} + \int_{i-1}^i \dot{\epsilon}_c dt \quad (4)$$

in which

$\dot{\epsilon}_c$  creep strain rate, percent/hr

$t$  time, hr

The creep rate is calculated by using the assumption that creep rate and rupture time are inversely proportional for the same stress and temperature. This simplifying assumption is consistent with creep-rate data on Nimonic 90 at relative high stress levels (ref. 1). The constant of proportionality between the creep rate and the inverse of the rupture time is assumed to depend on the temperature, or

$$\dot{\epsilon}_c(T, S) = \frac{K(T)}{t_r(T, |S|)} \times \frac{|S|}{S} \quad (5)$$

in which

$K$  known function of temperature, percent

$t_r$  time to rupture, hr

In this investigation, the rupture times  $t_r$  are calculated from the values of stress and temperature by using the following equation developed in reference 1:

$$\log(t_r) = A_T + B \log(|S|) + C|S| + DS^2 \quad (6)$$

in which

$\log$  logarithm to the base 10

$A_T$  temperature-dependent parameter, interpolated from a table of values

$B, C, D$  curve-fit constants, independent of temperature

The derivation of equation (6) is given in reference 1.

The integral in equation (4) is evaluated by using a standard Runge-Kutta technique, as explained in the appendix.

### Step 4: Calculation of Cyclic Creep Life

The calculation of accumulated creep damage is performed at the end of each time increment  $\Delta t$  by using the following equations (see fig. 4):

$$\Delta\varphi_c = \sum_0^{t_1} \frac{\Delta t}{t_r} \quad (7a)$$

and

$$\sum \Delta\varphi_c = 1 \text{ at failure} \quad (7b)$$

in which

$\varphi_c$  creep damage per cycle

$t_1$  duration of 1 cycle, hr

$t_r$  creep-rupture time at  $|S|$  and  $T$ , the average stress magnitude and temperature during  $\Delta t$ , hr

This is the so-called "linear damage rule" or "life-fraction rule" originally proposed by Robinson (ref. 5) to account for temperature variations during conventional creep. It was later modified by Taira (ref. 6) through the addition of the absolute-value sign to the

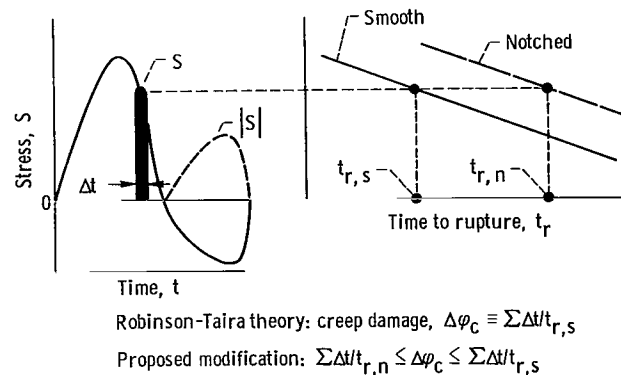


Figure 4. - Linear creep damage theory.

stress in order to give full weight to damage by compressive stresses. The role of compressive stress in causing creep damage is discussed further in this report, and a tentative hypothesis on the subject is proposed.

Over the years the simple linear damage rule has been very useful in estimating creep life under nonsteady conditions of stress and/or temperature. However, the damage fractions  $\Delta t/t_r$  are assumed to be independent of the strain history of the material. Thus, no distinction is made between a test with net strain (such as a conventional creep-rupture test) and one without net strain (such as a strain-cycling test). A simple modification to equations (7) was proposed in references 1 and 2 to account for some of the observed effects of net strain.

To derive this modification to equations (7), the assumption is first made that net strain is potentially detrimental to creep-rupture life, because it can lead to increasing true stress and tensile instability. Then, for a given nominal stress and temperature, it is assumed that a smooth creep specimen will have the shortest possible life, because such a specimen experiences the maximum amount of necking and, therefore, net strain. It is further assumed that a mildly notched creep specimen can be used to approximate the increase in creep-rupture life which can be expected if net strain is eliminated. At theoretical stress-concentration factors of 2 to 4 many alloys experience notch-strengthening. Rupture times are often considerably longer than those for smooth specimens at the same nominal stress and temperature. The triaxial stress state at the notched section severely limits necking and thereby substantially reduces net strain. It might be said that the beneficial effects of reducing creep strain more than offset the detrimental effects of the moderate stress concentration at the notch. On the basis of these assumptions, the rupture time in equation (7a) may vary between limits as follows:

$$t_{r, s} \leq t_r \leq t_{r, n} \quad (7c)$$

in which the subscripts *s* and *n* designate conventional creep-rupture data obtained with smooth and notched specimens, respectively. In this way, upper and lower bounds on life are calculated. In the case of actual notch-weakening ( $t_{r, n} < t_{r, s}$ ) only the smooth rupture time is used. The thermal-fatigue specimens are not notched; therefore, the detrimental effects of the stress-concentration should not be included. Notch-weakening simply indicates that any benefit to be derived from reducing net strain can be neglected. Equations (7a) to (7c) define what is called the "modified Robinson-Taira theory" for calculating cyclic creep damage. These equations depend only on the instantaneous values of stress and temperature, and they can therefore be applied to any cycle, however irregular or intricate. This flexibility is particularly useful for the life analysis of components which have complex service cycles.

The application of equations (7) is illustrated in figure 4. The stress *S* is the abso-

lute value of the average stress during the time increment  $\Delta t$ . The rupture times for smooth and notched specimens are then determined from equation (6) for this stress level acting continuously at the average temperature during  $\Delta t$ , and these quantities are designated as  $t_{r,s}$  and  $t_{r,n}$ , respectively. The increment of creep damage during  $\Delta t$  is then assumed to be greater than or equal to the fraction  $\Delta t/t_{r,n}$  and less than or equal to the fraction  $\Delta t/t_{r,s}$ . The accumulated creep damage at failure is assumed to be 1, so the theoretical number of cycles, each with duration  $t_1$ , which would cause cyclic creep failure is

$$\left. \begin{aligned}
 N_f &\geq \frac{1}{\sum_0^{t_1} \frac{\Delta t}{t_{r,s}}} \quad \text{or} \quad \frac{1}{\int_0^{t_1} \frac{dt}{t_{r,s}}} \\
 \text{and} \\
 N_f &\leq \frac{1}{\sum_0^{t_1} \frac{\Delta t}{t_{r,n}}} \quad \text{or} \quad \frac{1}{\int_0^{t_1} \frac{dt}{t_{r,n}}}
 \end{aligned} \right\} \quad (8)$$

in which  $N_f$  is the number of cycles to failure.

### Step 5: Calculation of Low-Cycle Fatigue Life

The number of cycles required for conventional low-cycle fatigue failure is calculated from the following empirical equations which comprise the Method of Universal Slopes (ref. 6):

$$\Delta\epsilon_m \equiv \Delta\epsilon_e + \Delta\epsilon_i \quad (9a)$$

$$\Delta\epsilon_e = 3.5 \frac{UTS}{E} N_f^{-0.12} \quad (9b)$$

$$\Delta\epsilon_i = 100 D_t^{0.6} N_f^{-0.6} \quad (9c)$$

in which

- $\Delta\epsilon$  strain range, percent
- m, e, i mechanical, elastic, and inelastic, respectively
- $N_f$  number of cycles to failure
- UTS ultimate tensile strength, ksi ( $\text{kN}/\text{cm}^2$ )
- E Young's Modulus, ksi/percent ( $\text{kN}/\text{cm}^2/\text{percent}$ )
- $D_t$  tensile ductility,  $-\ln(1 - \text{RA}/100)$
- RA reduction of area, percent

Figure 5 illustrates how equations (9) are used to predict low-cycle fatigue life for the

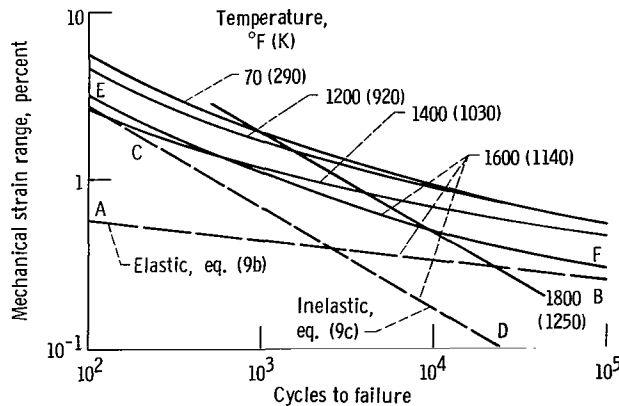


Figure 5. - Conventional fatigue resistance of Nimonic 90, predicted by Method of Universal Slopes.

alloy Nimonic 90. Line AB is the predicted relation between the elastic strain range and cycles to failure at  $1600^{\circ}\text{F}$ , while line CD is the relation between the inelastic strain range and cycles to failure. In this simplified analysis, the slopes of  $-0.12$  and  $-0.6$  on full logarithmic coordinates are used for all metals, which leads to the designation "universal" slopes. The sum of the ordinates from lines AB and CD produces the line EF, allowing a prediction of life solely from the mechanical strain range. The analyst need not determine the individual elastic and inelastic components, which are often more difficult to compute and subject to greater error than the mechanical strain range.

Equations (9) were originally developed to describe fatigue behavior which is relatively independent of time effects. Cyclic frequency and creep were assumed to be variables of minor importance. These same assumptions are inherent when equations (9) are used to calculate high-temperature life. As the test temperature is raised, a fatigue failure without any creep effects becomes more of an idealization. In reference 16, Manson

discussed the effects of creep on fatigue and proposed a simple modification to the Method of Universal Slopes which leads to a more realistic prediction of high-temperature fatigue life. As a first approximation, various creep effects were assumed to combine to reduce high-temperature life to about one-tenth the value computed from equations (9). This "10% rule" was evaluated further in reference 17 and was found to provide a reasonable lower bound on life for a variety of alloys, test temperatures, and cyclic frequencies. Thus, equations (9) and the 10% rule can be used to predict cycle-dependent lives neglecting and including creep effects, respectively.

For the Glenny-type tests, the strain ranges are defined by the minimum and maximum strains which occur during the heating and cooling half-cycles, respectively. When temperatures vary during a cycle, it has been recommended that a conservative approach be taken, namely that the temperature which leads to the shortest calculated life be used. This procedure was followed in this investigation, and generally produced the best correlation between theory and experiment of several assumptions which could be used to obtain an "equivalent" temperature.

## RESULTS AND DISCUSSION

Comparisons of calculated and observed thermal-fatigue lives are presented in three groups: (1) thermal fatigue of standard disk specimens, (2) thermal fatigue of oversize disk specimens with and without core-cooling, and (3) combined results.

In order to perform the complete five-step analysis which was summarized in the preceding sections, the following material properties were required:

- (1) Thermal conductivity
- (2) Specific heat
- (3) Density
- (4) Mean coefficient of thermal expansion
- (5) Young's Modulus (dynamic)
- (6) Yield strength
- (7) Ultimate tensile strength
- (8) Reduction of area
- (9) Creep-rupture strength
- (10) Creep strain rate

These quantities are given for Nimonic 90 in table I.

The ratio of the creep-rate parameter  $K$  in equation (5) to the tensile elongation was found to be 0.14 both at 1400<sup>o</sup> and 1800<sup>o</sup> F (1030 and 1250 K). These two temperatures represent the extremes in elongation for this alloy, so the same ratio of 0.14 was assumed to apply at all temperatures, leading to the values of  $K$  shown in table I.

TABLE I. - MECHANICAL AND THERMAL PROPERTIES OF NIMONIC 90

(a) U. S. customary units

Property	Temperature, T, °F								
	70	600	1000	1200	1400	1600	1800	2000	2100
Ultimate tensile strength, UTS, ksi	179	165	160	151	122	65	----	----	----
Yield strength, S <sub>y</sub> , ksi	100	99	86	84	78	63	29	5	----
Reduction of area, RA, percent	41	44	42	31	14	22	----	----	----
Creep-rate parameter, K, percent	---	---	3.8	1.7	1.6	3.4	9.6	20.0	22.0
Creep-rupture temperature parameter, log(hr):									
Smooth, A <sub>T, s</sub>	---	---	15.00	12.70	10.40	7.92	4.39	1.92	1.32
Notched, A <sub>T, n</sub>	---	---	15.26	12.96	10.66	8.18	4.88	2.41	1.81
Creep-rupture time (S = stress, ksi), log(hr):									
Smooth, log(t <sub>r, s</sub> )	A <sub>T, s</sub> - 4.95 log(S) + 0.00660 S - 0.000277 S <sup>2</sup>								
Notched, log(t <sub>r, n</sub> )	A <sub>T, n</sub> - 3.68 log(S) - 0.0669 S + 0.000206 S <sup>2</sup>								
Young's Modulus (dynamic), E, ksi/percent	$332 - 88\left(\frac{T}{1800}\right) - 36\left(\frac{T}{1800}\right)^3$								
Mean coefficient of thermal expansion (from 70° F), $\bar{\alpha}$ , percent/°F	$\left[6.30 + 2.40\left(\frac{T}{1800}\right) + 1.75\left(\frac{T}{1800}\right)^3\right] \times 10^{-4}$								
Thermal conductivity, k, Btu-in./ft <sup>2</sup> /hr/°F	$66 + 91\left(\frac{T}{1800}\right) + 17\left(\frac{T}{1800}\right)^3$								
Specific heat, $\gamma$ , Btu/lb/°F	0.108 + 0.0000244 T								
Density, $\rho$ , lb/in. <sup>3</sup>	0.296								

TABLE I. - Concluded. MECHANICAL AND THERMAL PROPERTIES OF NIMONIC 90

(b) SI units

Property	Temperature, T, K								
	290	590	810	920	1030	1140	1250	1360	1420
Ultimate tensile strength, UTS, kN/cm <sup>2</sup>	123	114	110	104	84	45	----	----	----
Yield strength, S <sub>y</sub> , kN/cm <sup>2</sup>	69	68	59	58	54	43	20	3.5	----
Reduction of area, RA, percent	41	44	42	31	14	22	----	----	----
Creep-rate parameter, K, percent	---	---	3.8	1.7	1.6	3.4	9.6	20.0	22.0
Creep-rupture temperature parameter, log(hr):									
Smooth, A <sub>T, s</sub>	---	---	14.20	11.90	9.20	7.12	3.59	1.12	0.52
Notched, A <sub>T, n</sub>	---	---	14.66	12.36	10.06	7.58	4.28	1.81	1.21
Creep-rupture time (S = stress, kN/cm <sup>2</sup> ), log(hr):									
Smooth, log(t <sub>r, s</sub> )	A <sub>T, s</sub> - 4.95 log(S) + 0.00957 S - 0.000583 S <sup>2</sup>								
Notched, log(t <sub>r, n</sub> )	A <sub>T, n</sub> - 3.68 log(S) - 0.0970 S + 0.000433 S <sup>2</sup>								
Young's Modulus (dynamic), E, kN/cm <sup>2</sup> /percent	229 - 61 $\left(\frac{T - 256}{1000}\right)$ - 25 $\left(\frac{T - 256}{1000}\right)^3$								
Mean coefficient of thermal expansion (from 290 K), $\bar{\alpha}$ , percent/K	$\left[ 11.3 + 4.31 \left(\frac{T - 256}{1000}\right) + 3.15 \left(\frac{T - 256}{1000}\right)^3 \right] \times 10^{-4}$								
Thermal conductivity, K, W/m/K	9.5 + 13.1 $\left(\frac{T - 256}{1000}\right)$ + 2.4 $\left(\frac{T - 256}{1000}\right)^3$								
Specific heat, $\gamma$ , J/g/K	0.452 + 0.000184(T - 256)								
Density, $\rho$ , g/cm <sup>3</sup>	8.20								

### Standard Disk Specimens

Preliminary calculations. - In figures 6 and 7, calculated and observed temperatures are compared for a standard disk specimen during rapid heating and cooling between 70° and 1690° F (290 and 1190 K). Good agreement was obtained by using surface heat-transfer coefficients of 200 and 130 Btu per square foot per hour per °F (1130 and 740 W/m<sup>2</sup>/K) for heating and cooling, respectively. These are the same coefficients reported in reference 7. In order to match observed temperature gradients in the disk, it was necessary to reduce the thermal conductivity to 70 percent of the nominal value given in table I. This reduced conductivity probably results from the lumped-parameter approximations in the heat-transfer analysis.

Figure 8 shows the mechanical strain cycle at the periphery as calculated from the transient temperatures, assuming completely elastic behavior. The minimum and maxi-

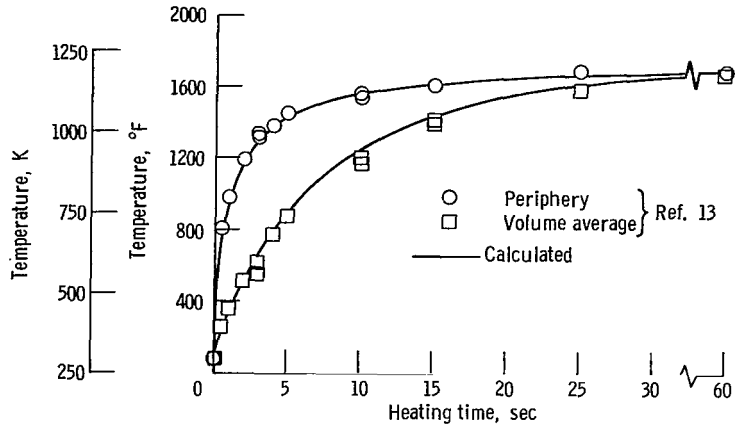


Figure 6. - Calculated and observed temperatures during heating of standard disk specimen of Nimonic 90. Temperature range, 70° F → 1690° F (290 K → 1190 K).

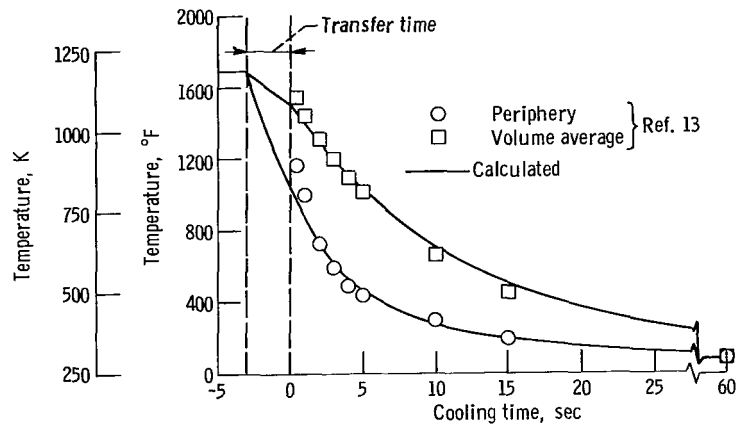


Figure 7. - Calculated and observed temperatures during cooling of standard disk specimen of Nimonic 90. Temperature range, 1690° F → 70° F (1190 K → 290 K).

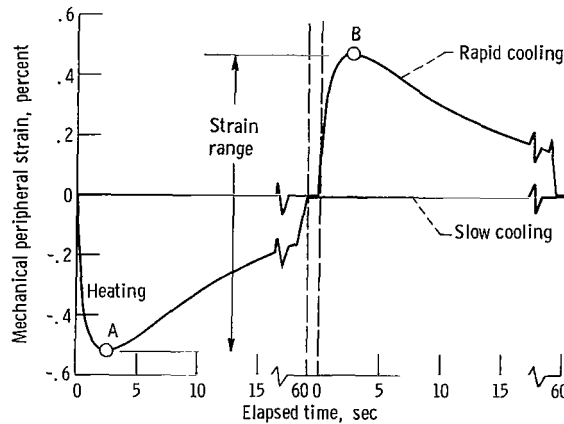
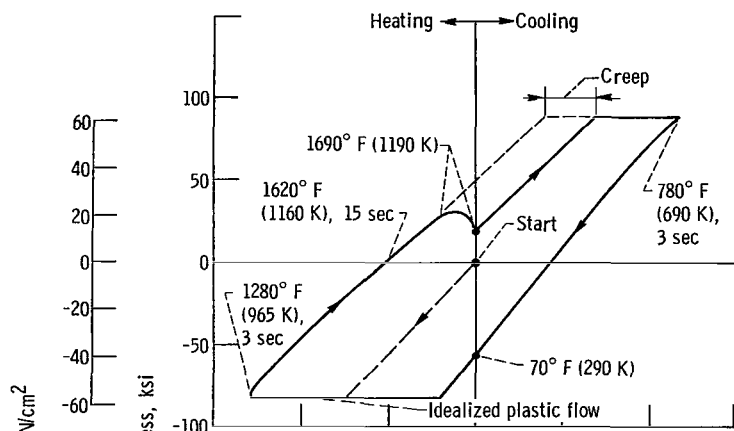


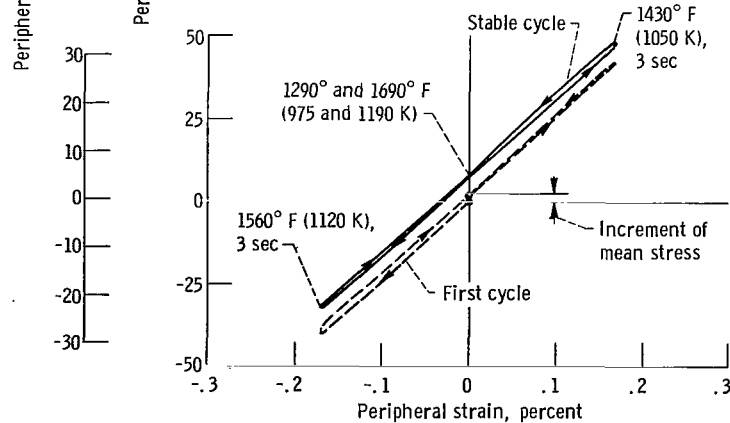
Figure 8. - Calculated peripheral strain in standard disk specimen of Nimonic 90. Temperature range, 70° F → 1690° F (290 K → 1190 K).

imum values occur within a few seconds after the start of rapid heating and cooling, respectively. The mechanical strains become asymptotic to zero with time because of the uniform temperature conditions approached in the disk. During slow cooling, mechanical strain is assumed to remain zero at all times. The strain range for rapid heating and rapid cooling is approximately twice that for rapid heating and slow cooling, which leads to considerably different calculated fatigue lives for the two conditions.

Figure 9(a) illustrates a typical stress-strain hysteresis loop containing time-independent plastic flow as well as creep strain. The minimum and maximum stresses were obtained from the yield strength of the alloy (table I) at temperatures of 1280° and



(a) With plastic flow. Temperature range, 70° F ≠ 1690° F (290 K ≠ 1190 K).



(b) Without plastic flow. Temperature range, 1290° F ≠ 1690° F (975 K ≠ 1190 K).

Figure 9. - Typical stress-strain hysteresis loops for standard disk specimens of Nimonic 90.

780° F (970 and 690 K), respectively. In this way, the critical extreme conditions in the cycle are consistent combinations of stress, strain, and temperature. At the start of heating, compressive peripheral stress is induced which quickly reaches the yield strength of the alloy and remains there until 3 to 5 seconds have elapsed. Thereafter, elastic unloading to zero stress is accomplished in another 12 seconds, followed by re-loading in tension. Creep strain is continuously occurring during both the compressive and tensile portions of the cycle. However, most of the creep strain occurs during the tensile part of the heating half-cycle. The residual tensile stress resulting from the previous compressive plastic strain is considerably reduced by creep relaxation, as shown in figure 9(a).

During rapid cooling, peripheral stress reaches and remains at the yield for 3 to 5 seconds and then unloads to a residual compression condition. Because of lower temperatures, creep during cooling is not significant. Successive cycles repeat the pattern of the first cycle because tensile and compressive inelastic strains become, and remain, equal in magnitude.

A second type of stress-strain loop is shown in figure 9(b). In this type, the temperature range during the cycle is not sufficient to cause instantaneous plastic flow. On the first cycle, more creep occurs in compression during heating than in tension during cooling. Therefore, the second cycle is not a duplicate of the first but contains higher stresses for the same strains. This increase in average stress with cycling continues until tensile and compressive creep strains balance and the cycle begins and ends at the same stress. For this reason, "elastic" cycles require an iterative calculation process which is not necessary when plastic strain is present.

Final results. - Calculated and observed cyclic lives are compared in figures 10 to 15 for thermal-fatigue tests on the standard disk specimen of Nimonic 90 alloy. The effects on life of the following parameters are shown: (1) assumed yield stress, (2) duration of the heating half-cycle, (3) minimum temperature for a constant maximum temperature, (4) maximum temperature for a constant minimum temperature, (5) maximum temperature for a constant temperature range, and (6) heating and cooling rates. The observed number of cycles to crack initiation was determined by averaging the cycle numbers of the last inspection without cracking and the first inspection with cracks. Most of the results are the average lives of several specimens.

In figure 10, the calculated number of cycles which cause cracking is presented as a function of the assumed yield stress for the cycle which was shown in figure 9(a). The upper and low bounds of the band are lives calculated from equation (8) by using the rupture strength of smooth and notched specimens, respectively. As the assumed yield stress decreases in magnitude, creep damage during compression is reduced and tensile creep damage is increased. This occurs because higher tensile stresses are induced as the plastic strain in compression increases. At yield stresses less than 90 000 psi (62 kN/cm<sup>2</sup>), the increase in tensile damage is greater than the decrease in compressive

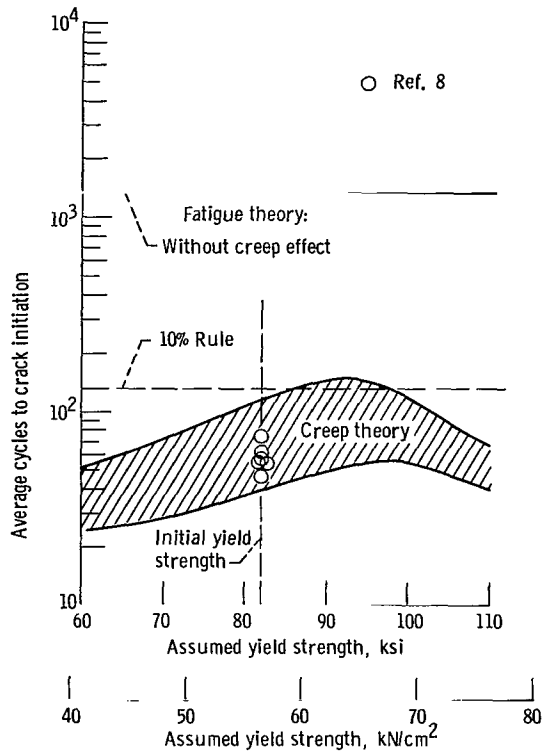


Figure 10. - Effect of assumed yield strength on calculated life. Standard disk specimen of Nimonic 90; temperature range, 70° F  $\approx$  1690° F (290 K  $\approx$  1190 K).

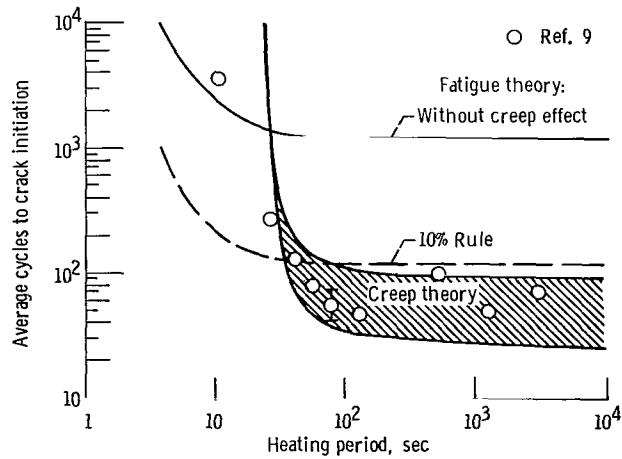


Figure 11. - Effect of the duration of the heating period on thermal-fatigue life. Standard disk specimen of Nimonic 90; temperature range, 70° F  $\approx$  1690° F (290 K  $\approx$  1190 K).

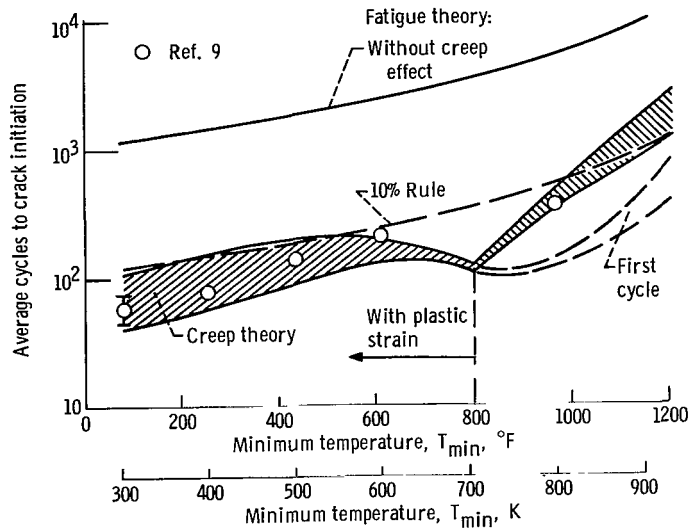


Figure 12. - Effect of minimum temperature on thermal-fatigue life. Standard disk specimen of Nimonic 90; temperature range,  $T_{\min} \approx 1690^{\circ}\text{F}$  ( $T_{\min} \approx 1190\text{ K}$ ).

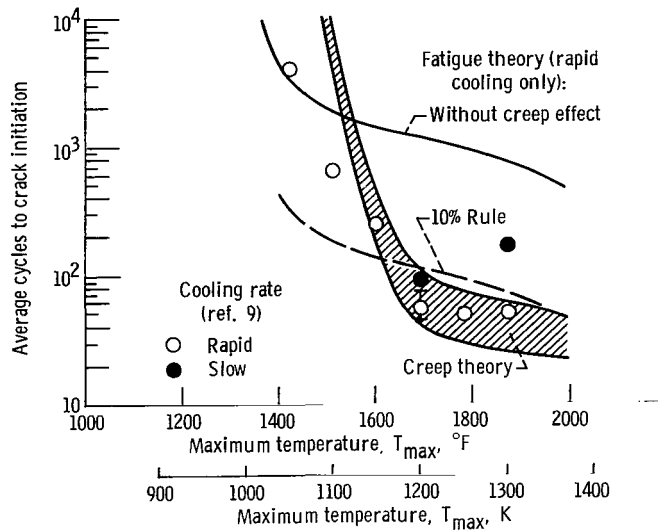


Figure 13. - Effect of maximum temperature on thermal-fatigue life with constant minimum temperature. Standard disk specimen of Nimonic 90; temperature range,  $70^{\circ}\text{F} \approx T_{\max}$  ( $290\text{ K} \approx T_{\max}$ ).

damage, causing a reduction in calculated lives. Thus, if compression is assumed to be as damaging as tension, the calculated cyclic life is relatively insensitive to errors in the assumed yield stress of the alloy for cycles which contain instantaneous plastic strain. Of course, cycles without plastic strain are also not affected by errors in yield strength. This leads to the conclusion that an accurate knowledge of the cyclic yield strength of the alloy is not always necessary. Therefore, the initial yield strength was used in all the remaining life calculations to establish minimum and maximum stresses in a given cycle.

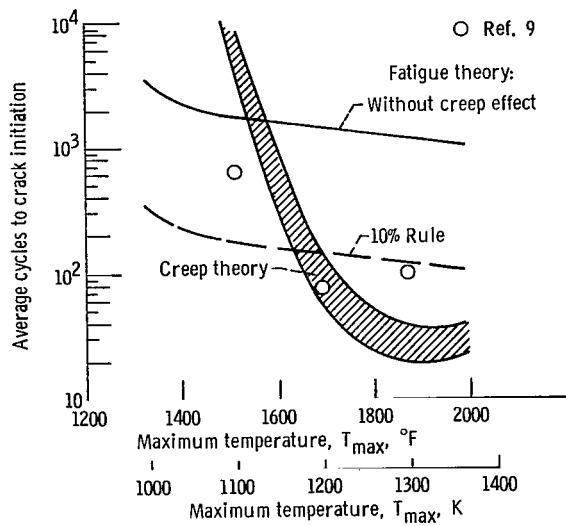


Figure 14. - Effect of maximum temperature on thermal-fatigue life with constant temperature range. Standard disk specimen of Nimonic 90; temperature range,  $T_{max} - 1440^\circ \text{F} \approx T_{max}$  ( $T_{max} - 1060 \text{ K} \approx T_{max}$ ).

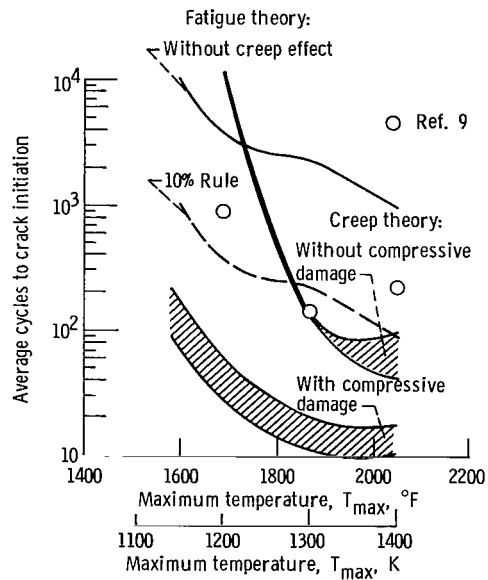


Figure 15. - Effect of compressive damage on calculated thermal-fatigue life under slow heating and rapid cooling conditions. Standard disk specimen of Nimonic 90; temperature range,  $70^\circ \text{F} \approx T_{max}$  ( $290 \text{ K} \approx T_{max}$ ).

Test results from reference 8 are plotted in figure 10 at a yield stress equal to the initial yield strength of the alloy. These results agree with the calculated life range, demonstrating the reasonableness of the concept that thermal fatigue can be a form of creep-rupture. Creep damage during the cooling half-cycle was negligible for these tests, so the assumed yield stress in tension was not an important parameter. The calculated low-cycle fatigue life for these tests without creep effects was about 2500 cycles, which emphasizes the dominant role of creep and the minor role of conventional fatigue in causing the thermal-fatigue cracks.

Figure 11 shows the effect of the duration of the heating half-cycle on the number of cycles to failure. During these tests, the heat-transfer coefficient was always the same, so the rate of heating did not change. Thus, the strain limits were approximately constant while the creep strain varied. The data from reference 9 are an average of three specimens and show a severe reduction in life as the heating period increases from 10 to 100 seconds and no significant change for longer periods. It can be seen that the lives calculated with the linear creep damage theory are in good agreement with these data. The estimated fatigue life agrees with the endurance of a 10-second immersion test. However, because longer immersion times do not significantly change the strain range for the complete cycle, approximately the same conventional fatigue life would be calculated for all heating times, which is inconsistent with the test results.

In figure 12, calculated and observed lives are compared for tests in which the maximum temperature was maintained at  $1690^{\circ}$  F ( $1190$  K) while the minimum temperature was varied. Both heating and cooling were rapid. It can be seen that lives calculated by the creep theory agree with the experimental data, while fatigue theory greatly overestimates the lives. The sharp change in calculated creep life at a minimum temperature of  $800^{\circ}$  F ( $700$  K) signifies the transition from cycles with plastic strain to cycles without such strain. It is apparent that errors in life calculation can result if the first-cycle stresses are used when plastic strain is absent. In general, large changes in minimum temperature are required to cause significant changes in cyclic life. This indicates a dominant role for the maximum temperature, which was held constant during this series of tests.

Considerably different behavior is observed when the minimum temperature is held at  $70^{\circ}$  F ( $290$  K) and the maximum temperature is changed. This behavior is shown in figure 13. Data from reference 9 show a sharp decrease in cyclic life as the maximum temperature is increased from  $1400^{\circ}$  to  $1700^{\circ}$  F ( $1030$  and  $1200$  K). For maximum temperatures above  $1700^{\circ}$  F ( $1200$  K), lives remain approximately constant if cooling is rapid, or they increase somewhat if the cooling rate is slow. The general trend of the test results is predicted by the creep theory, although the longer lives are overestimated. The minor effect of cooling rate is also predicted by this theory because most of the creep damage occurs during the heating half-cycle for maximum temperatures above  $1600^{\circ}$  F ( $1140$  K).

The fatigue theory indicates that, at maximum temperatures less than about 1460<sup>o</sup> F (1070 K), thermal-fatigue cracks would form in accordance with conventional low-cycle fatigue experience. However, the indicated fatigue resistance applies only to tests with rapid cooling. Slow cooling reduces the mechanical strain range by almost one-half, leading to calculated fatigue lives in excess of 10<sup>4</sup> cycles.

Figure 14 presents calculated and observed cycles to cracking for thermal-fatigue tests at a constant temperature range of 1440<sup>o</sup> F (1060 K). Comparison with figure 13 shows that the variation of cyclic life with maximum temperature was about the same, whether or not the temperature range was 1440<sup>o</sup> F (1060 K). This conclusion was reached experimentally by Glenny and Taylor (ref. 9) and is reaffirmed herein on the basis of calculated lives, but only for large temperature ranges. Apparently, the maximum temperature is a much more significant parameter in determining cyclic life than the temperature range when the range is large enough to cause plastic strain. However, figure 12 shows that for cycles without plastic strain, calculated life is sensitive to changes in minimum temperature, and therefore temperature range, when the maximum temperature is held constant.

To complete this analysis of thermal-fatigue tests on standard disks of Nimonic 90 alloy, figure 15 presents results for test cycles with rapid cooling but slow heating. At the end of the cooling half-cycle, the periphery of the disk specimen is in a stage of residual compression at zero mechanical strain and room temperature. During the slow heating to the maximum temperature, the residual compressive stress relaxes while the mechanical strain remains approximately zero. In effect, the stresses are annealed out of the disk. During this slow heating period, significant creep damage is accumulated if compressive stress is assumed to be fully as damaging as tensile stress of the same magnitude, as stated by equation (7a). However, figure 15 shows that lives calculated by using this assumption are an order of magnitude shorter than those observed experimentally. On the other hand, if damage is assumed to occur only during tension, agreement between experiment and theory is the same as that shown in figures 10 to 14 for rapid heating and cooling. This behavior is very similar to that observed here at Lewis. Cyclic creep-rupture tests of the "square wave" type were conducted on the cobalt-base alloy L-605 and on 316 stainless steel. In this type of test, equal magnitudes of stress are applied alternately in tension and compression, and the stress is held constant while the specimen creeps between fixed strain limits. The results of these tests are compared with monotonic creep-rupture time in figures 16(a) and (b). In these figures, nominal stress is plotted against rupture time. If only the time spent in tension is plotted for the cyclic tests, the data points fall within or very near the range bounded by smooth and notched monotonic strength. However, this range significantly underestimates the total cyclic rupture time, particularly for the L-605 alloy. Thus, figures 15 and 16 strongly indicate that compressive stress is not particularly damaging, at least when the mechanical strain rate is zero (conventional relaxation) or the stress rate is

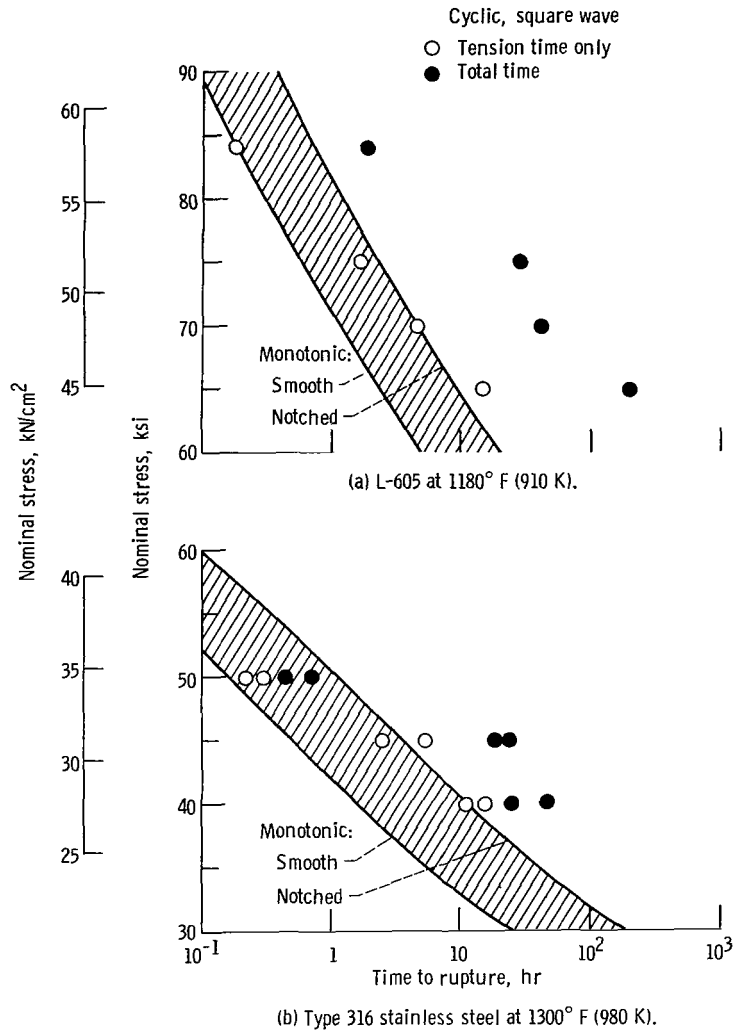


Figure 16. - Comparison of cyclic and monotonic creep-rupture lives.

zero (conventional creep).

On the other hand, the analysis of other test data indicates that compressive stresses can be damaging under other conditions of stress and strain rate. For example, when L-605 specimens were strain-cycled sinusoidally at constant temperature, calculated and observed lives agreed much better when compressive damage was included than when it was neglected (ref. 2). Another strong indication of compressive damage is shown in figure 17. In a series of tests reported in reference 18, Hastelloy X specimens were thermally and mechanically cycled in three ways: with temperatures and strains in phase, with temperatures and strains 180 degrees out of phase, and isothermally. The in-phase test produced tension at 1800<sup>o</sup> F (1260 K), while the out-of-phase tests contained compression at 1800<sup>o</sup> F (1260 K). Of course, the isothermal tests had both tension and com-

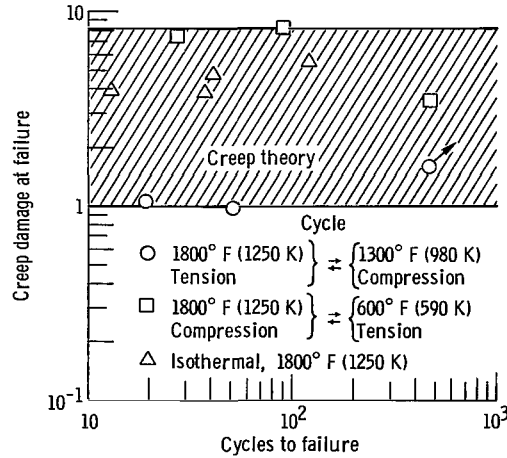


Figure 17. - Creep damage in Hastelloy X from combined strain and temperature cycling (ref. 18).

pression at 1800° F (1260 K). As shown in figure 17, the creep damage at failure, including all compressive damage, approaches approximately the same value for all three tests as lives approach 10<sup>3</sup> cycles. At this life, stresses are low enough so that conventional creep and relaxation in compression are small.

Apparently, equations (7) may require further modification to account for the actual stress and strain rates occurring in compression. The following tentative criterion is now proposed to determine if compressive stress causes creep damage:

During an increment of time, compressive stress causes creep damage if and only if the algebraic product of the stress rate and the mechanical strain rate is greater than zero.

Thus, equation (7c) might be rewritten as

$$\lambda t_{r, s} \leq t_r \leq \lambda t_{r, n}$$

in which

$$\lambda = \begin{cases} 1 & \text{for } S \geq 0 \\ 1 & \text{for } S < 0 \quad \text{and} \quad \dot{S}\dot{\epsilon}_m > 0 \\ \infty & \text{for } S < 0 \quad \text{and} \quad \dot{S}\dot{\epsilon}_m \leq 0 \end{cases}$$

and  $\dot{S}$  and  $\dot{\epsilon}_m$  are the stress and mechanical strain rates, respectively. The tentative nature of this hypothesis must be emphasized. Considerable testing would be required to establish its

validity. However, it does appear to be consistent with the high-temperature test data analyzed to date by the modified Robinson-Taira theory.

## Oversize Disk Specimens

Thermal-fatigue tests on oversize specimens with and without core-cooling (ref. 12) were conducted with a nominal temperature cycle of room temperature to 1690° F (1190 K) at a frequency of 1/8 cycle per minute. When core-cooling was used, it was necessary to raise the maximum bed temperature to 1725° F (1210 K) in order to maintain the periphery of the specimen at 1690° F (1190 K) during the steady-state periods.

The results of the transient temperature analysis for the core-cooled condition are shown in figure 18. In this case, three sets of data were considered: peripheral,

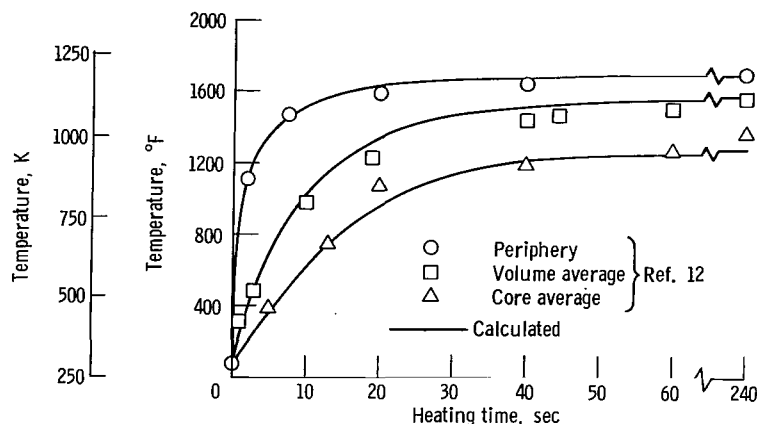


Figure 18. - Calculated and observed temperatures during heating of core-cooled disk specimen. Oversize disk specimen of Nimonic 90; temperature range, 70° F  $\approx$  1690° F (290 K  $\approx$  1190 K).

volume-average, and core temperatures. Only two variable quantities were used to fit calculated temperatures to these data: the bed and core heat-transfer coefficients. A good fit of the temperature data was obtained when the bed and core coefficients were 210 and 380 Btu per square foot per hour per °F (1190 and 2150 W/m<sup>2</sup>/K), respectively. Some deviations in the transient volume-average temperature and in the steady-state core temperature were noted. Also, it was necessary to reduce the boundary temperature for the heat-transfer analysis to 1710° F (1200 K) from the bed temperature of 1725° F (1210 K). This is not unrealistic because the bed temperature near the specimen may actually have been reduced somewhat by the cooled shaft supporting the specimen. The

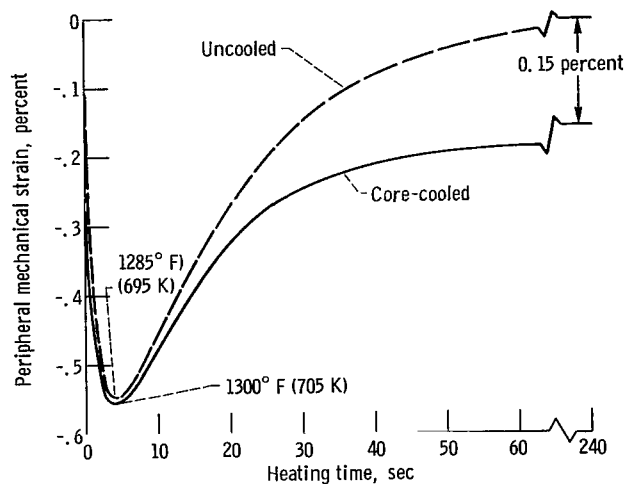


Figure 19. - Calculated peripheral strains, with and without core cooling. Oversize disk specimens of Nimonic 90; temperature range, 70° F  $\pm$  1690° F (290 K  $\pm$  1190 K).

same bed coefficient was used for the disk without core-cooling, but with the bed temperature of 1690° F (1190 K).

Figure 19 shows the variation of calculated peripheral strain during the heating half-cycle. In 4 seconds, both strain cycles reach minimum values with only minor differences in strain or temperature. Thus, core-cooling has had little effect on the transient part of the cycle. The major difference in peripheral strain between the core-cooled and the uncooled cycles is found during the steady-state period. In the uncooled disk, a uniform temperature is eventually reached throughout the specimen, and the mechanical strain therefore approaches zero. In contrast, the core-cooled disk has a temperature gradient even in the steady-state condition, and the hotter periphery sustains a steady compressive strain of about 0.15 percent at the end of the transient period.

The effect of this compressive strain on the stress cycle for the core-cooled disk is shown in figure 20. In this figure, the compressive yield strengths are assumed to maintain their first-cycle values of 82 000 psi (56 kN/cm<sup>2</sup>). No difference in the compressive stresses with and without core-cooling is observed for the first 10 seconds of the heating period. However, a major difference exists in the residual tension stresses. The residual compressive strain induced in the periphery by core-cooling causes a significant reduction in tensile stress. Without core-cooling, tensile stress reaches a peak value of 31 000 psi (21 kN/cm<sup>2</sup>), followed by considerable relaxation. On the other hand, core-cooling limits the tensile stress to values less than 16 000 psi (11 kN/cm<sup>2</sup>) with very little relaxation.

Figures 21(a) and (b) show the results of the thermal-fatigue tests on the oversize

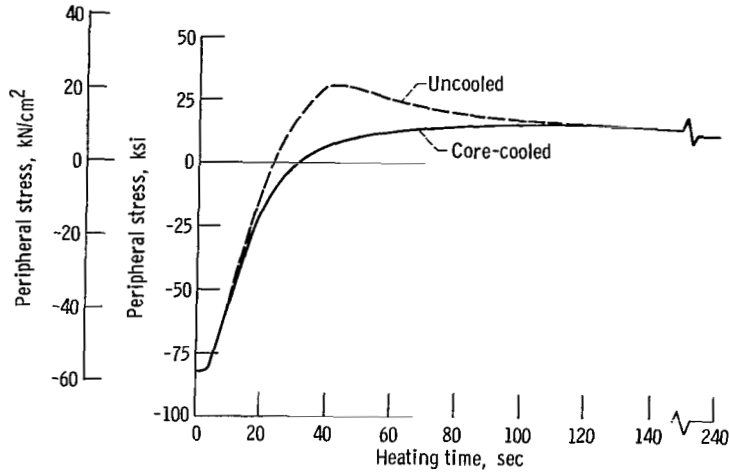


Figure 20. - Calculated peripheral stresses, with and without core-cooling. Oversize disk specimen of Nimonic 90; temperature range,  $70^\circ\text{F} \approx 1690^\circ\text{F}$  ( $290\text{K} \approx 1190\text{K}$ ).

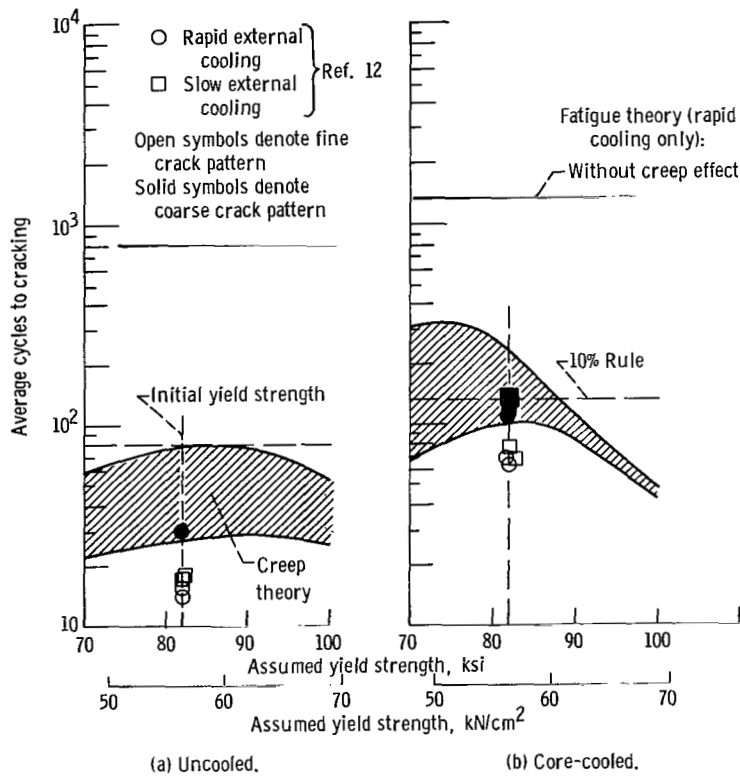


Figure 21. - Effect of core-cooling on thermal-fatigue life. Oversize disk specimens of Nimonic 90; temperature range,  $70^\circ\text{F} \approx 1690^\circ\text{F}$  ( $290\text{K} \approx 1190\text{K}$ ).

disk specimens with and without core-cooling, respectively. Two test cycles and two failure criteria were used. The test cycles contained either rapid or slow cooling on the outside of the specimens, and failure was judged by either a fine or a coarse pattern of cracking, termed the first and second standards, respectively. It can be seen that the rate of external cooling did not significantly affect cyclic life, even though the mechanical strain ranges differed by a factor of almost 2. This was predicted by the creep theory because almost all creep damage occurs during the heating half-cycle, which in this case is not altered by the cooling rate. Calculated and observed lives are in agreement, both in the actual number of cycles and in the ratio of core-cooled to uncooled lives. The lower bound on calculated life agrees better with the data. Using the lower bounds for the two conditions, it was calculated that core-cooling would improve life by a factor of 3.9, which compares favorably with an observed improvement of a factor of 3.8 to 4.5 for the coarse and fine cracks, respectively. It was also observed that the periods of crack propagation from fine cracks to coarse cracks were in the ratio of 3 to 1. This may indicate that in thermal fatigue, crack propagation, as well as crack initiation, is governed by creep damage.

### Combined Results

Figure 22 is a plot of observed cycles to crack initiation as a function of calculated

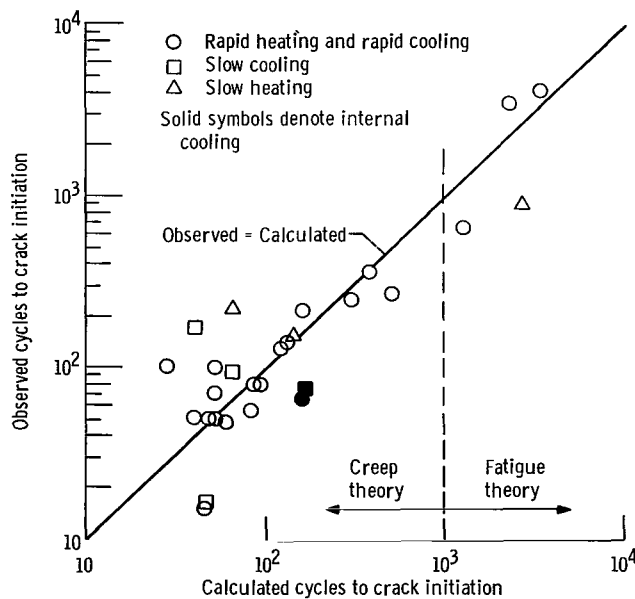


Figure 22. - Comparison between average observed and average calculated thermal-fatigue lives for Nimonic 90 disk specimen.

lives and summarizes the thermal-fatigue data presented earlier. Twenty-eight different thermal cycles are represented. In most cases, the results plotted are the average of two or more specimens. The calculated lives are either the average of the upper and lower bounds given by the creep theory or the lives calculated by the Method of Universal Slopes without any creep effects included, whichever is shorter. Considering both creep and fatigue damage by the methods discussed in this report, cyclic creep was found to be the dominant failure mechanism in 24 of the 28 cases analyzed. Fatigue was dominant in two cases, and both mechanisms were important in two cases. For these disk specimens of Nimonic 90, lives below 1000 cycles were governed by cyclic creep, while those above 1000 cycles were governed by fatigue, regardless of the thermal cycle applied. However, this crossover life could easily change with the addition of external loads or changes in geometry.

## CONCLUDING REMARKS

Thermal-fatigue tests of the Glenny type have been analyzed by using a modification of the Robinson-Taira cumulative damage theory and the empirical Method of Universal Slopes. To perform this life analysis, it was necessary to calculate transient temperatures, strains, creep damage, and conventional fatigue damage. The results are very promising; it appears that the simple creep and fatigue theories used in this investigation are sufficient for the analysis and prediction of thermal-fatigue life. Therefore, a practical method has been developed for predicting crack initiation in high-temperature components subjected to arbitrary thermal-mechanical cycling.

Three major topics have been investigated: (1) the importance of creep in thermal fatigue, (2) improvement in the correlation between theory and experiment, and (3) simplification of the stress analysis of thermal-fatigue specimens. Specific conclusions can be drawn for each topic. While conclusions concerning the importance of creep are quite well substantiated by the results of this study, the second and third topics have not yet been thoroughly investigated. Therefore, the conclusions concerning correlation of theory with experiment and simplification of stress analysis require further study and possible modification.

### 1. Importance of creep in thermal fatigue:

a. Considering both creep and fatigue damage, cyclic creep-rupture is the dominant failure mode in 24 of the 28 different thermal-fatigue tests analyzed in this investigation.

b. The linear damage rule for creep (Robinson-Taira theory) in its simplest form is capable of predicting the general effects on thermal-fatigue life of changes in such parameters as the temperature limits, heating and cooling rates, hold times, and

geometry. This theory is not restricted to a specific thermal or mechanical cycle, but can be applied to cycles of arbitrary form.

c. Use of conventional fatigue equations which relate cyclic life to strain range without specifically accounting for creep effects can lead to extremely unconservative life predictions. This is particularly true in the short and intermediate life ranges in which cyclic creep is generally the mode of failure. Fatigue may become dominant at longer lives, in which case the creep theory would be unconservative. Hence, accurate life prediction over a wide range of lives requires the use of both theories.

## 2. Improved correlation between theory and experiment:

a. The Robinson-Taira theory can be modified by using conventional creep-rupture data from both smooth and mildly notched ( $K_t = 2$  to 4) specimens to represent rupture times with and without net strain, respectively. In this way, lower and upper bounds are defined for theoretical lives which may agree better with a variety of thermal-fatigue data than a single prediction which neglects the effect of net strain on rupture time.

b. The rate of creep damage is generally governed by the absolute value of the stress, as well as the temperature. However, when creep at constant stress or relaxation at constant strain occurs in compression, damage apparently should be neglected. A tentative criterion is suggested to determine whether or not to include compressive damage: If and only if the algebraic product of the stress rate and the mechanical strain rate is greater than zero during a time interval, compressive damage should be included for that interval.

## 3. Simplified stress analysis:

a. The assumptions of (1) the invariance of total strain with plastic flow and creep and (2) the inverse proportionality of the creep strain rate and rupture time lead to the calculation of thermal stresses in a greatly simplified manner with adequate accuracy.

b. Accurate knowledge of changes in alloy yield strength caused by cycling is apparently not necessary for calculating thermal-fatigue life.

The value of the proposed thermal-fatigue theory will be determined by the extent to which it can serve as a guide for the development of materials and the design of components with improved thermal-fatigue resistance. This investigation indicates that research for the purpose of predicting and eventually improving thermal-fatigue life should be focused on the calculation and reduction of creep damage.

Lewis Research Center,  
National Aeronautics and Space Administration,  
Cleveland, Ohio, August 6, 1969,  
129-03.

## APPENDIX - INTEGRATION OF CREEP STRAIN RATE

The integral in equation (4) was evaluated by using the standard Runge-Kutta technique with fourth-order accuracy as follows: Let

$$\Delta t = t_i - t_{i-1}$$

$$\tau_1 = t_{i-1}$$

$$\tau_2 = t_{i-1} + \frac{\Delta t}{2} = \tau_3$$

$$\tau_4 = t_i$$

Then

$$\int_{i-1}^i \dot{\epsilon}_c dt = \frac{1}{6} (b_1 + 2b_2 + 2b_3 + b_4)$$

in which

$$b_j = \Delta t \dot{\epsilon}_c(T_j, S_j) \quad j = 1, 4$$

$$T_j = T(\tau_j)$$

$$S_j = E_j(\epsilon_{o,j} - \epsilon_{p,j} - \epsilon_{c,j} - \epsilon_{T,j})$$

$$E_j = E(T_j)$$

$$\epsilon_{o,j} = \epsilon_o(\tau_j)$$

$$\epsilon_{c,j} = \epsilon_{c,j-1} + \Delta \epsilon_j$$

$$\Delta \epsilon_1 = 0$$

$$\Delta\epsilon_2 = \frac{b_1}{2}$$

$$\Delta\epsilon_3 = \frac{b_2}{2}$$

$$\Delta\epsilon_4 = b_3$$

$$\epsilon_{p,j} = \epsilon_{p,j-1}$$

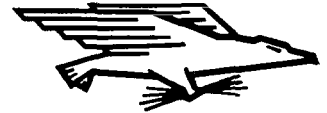
$$\epsilon_{T,j} = \epsilon_T(\tau_j)$$

## REFERENCES

1. Spera, David A.: A Linear Creep Damage Theory for the Thermal Fatigue of Materials. Ph. D. Thesis, University of Wisconsin, 1968.
2. Spera, D. A.: The Calculation of Creep Damage During Elevated Temperature, Low-Cycle Fatigue. Presented at ASM Materials Engineering Congress and Exposition, Detroit, Mich., Oct. 14-17, 1968.
3. Spera, David A.: The Calculation of Thermal-Fatigue Life Based on Accumulated Creep Damage. Presented at ASME Gas Turbine Conference and Products Show, Cleveland, Ohio, Mar. 9-13, 1969.
4. Howe, P. W. H.: Mathematical Techniques Applying to the Thermal Fatigue Behaviour of High Temperature Alloys. Aeron. Quart., vol. 13, pt. 4, Nov. 1962, pp. 368-396.
5. Robinson, Ernest L.: Effect of Temperature Variation on the Long-Time Rupture Strength of Steels. Trans. ASME, vol. 74, no. 5, July 1952, pp. 777-781.
6. Taira, S.: Lifetime of Structures Subjected to Varying Load and Temperature. Creep in Structures. Nicholas J. Hoff, ed., Academic Press, 1962, pp. 96-124.
7. Manson, S. S.: Fatigue: A Complex Subject - Some Simple Approximations. Experimental Mech., vol. 5, no. 7, July 1965, pp. 193-226.
8. Glenny, E.; Northwood, J. E.; Shaw, S. W. K.; and Taylor, T. A.: A Technique for Thermal-Shock and Thermal-Fatigue Testing Based on the Use of Fluidized Solids. J. Inst. Metals, vol. 87, 1958-59, pp. 294-302.
9. Glenny, E.; and Taylor, T. A.: A Study of the Thermal-Fatigue Behaviour of Metals. J. Inst. Metals, vol. 88, 1959-60, pp. 449-461.
10. Glenny, E.: The Influence of Specimen Geometry on Thermal-Fatigue Behaviour. Thermal and High-Strain Fatigue. The Metals and Metallurgy Trust, London, 1967, pp. 346-363.
11. Franklin, A. W.; Heslop, J.; and Smith, R. A.: Some Metallurgical Factors Influencing the Thermal-Fatigue Resistance of Wrought Nickel- and Chromium-Base High-Temperature Alloys. J. Inst. Metals, vol. 92, 1963-64, pp. 313-322.
12. Roberts, J. T.: Comparative Thermal Fatigue Tests on Nimonic 90 Tapered Disk Specimens With and Without Internal Air Cooling. Rep. NGTE-M-366, National Gas Turbine Establishment, Sept. 1963.
13. Shaw, S. W. K.: Transient Thermal Strains in Tapered Disks. Met. Dept. Note No. 347, National Gas Turbine Establishment, 1958.

14. Manson, S. S.: Determination of Elastic Stresses in Gas-Turbine Disks. NACA Rep. 871, 1947.
15. Mendelson, A.; and Manson, S. S.: Practical Solution of Plastic Deformation Problems in Elastic-Plastic Range. NASA TR R-28, 1959.
16. Manson, S. S.: Interfaces Between Fatigue, Creep, and Fracture. Int. J. Fracture Mech., vol. 2, no. 1, Mar. 1966, pp. 327-363.
17. Manson, S. S.; and Halford, G.: A Method of Estimating High-Temperature Low-Cycle Fatigue Behaviour of Materials. Thermal and High Strain Fatigue. The Metals and Metallurgy Trust, London, 1967, pp. 154-170.
18. Carden, A. E.; and Slade, T. B.: Low Cycle Fatigue of Hastelloy X. Presented at the 71st ASTM Annual Meeting, San Francisco, Calif., June 23-28, 1968.

FIRST CLASS MAIL



POSTAGE AND FEES PAID  
NATIONAL AERONAUTICS AND  
SPACE ADMINISTRATION

140 001 57 51 305 69273 00903  
AIR FORCE WEAPONS LABORATORY/WLIL/  
KIRTLAND AIR FORCE BASE, NEW MEXICO 87117

ALL E. CO. DONOR. CHIEF, TECH. LIBRARY

POSTMASTER: If Undeliverable (Section 158  
Postal Manual) Do Not Return

*"The aeronautical and space activities of the United States shall be conducted so as to contribute . . . to the expansion of human knowledge of phenomena in the atmosphere and space. The Administration shall provide for the widest practicable and appropriate dissemination of information concerning its activities and the results thereof."*

— NATIONAL AERONAUTICS AND SPACE ACT OF 1958

## NASA SCIENTIFIC AND TECHNICAL PUBLICATIONS

**TECHNICAL REPORTS:** Scientific and technical information considered important, complete, and a lasting contribution to existing knowledge.

**TECHNICAL NOTES:** Information less broad in scope but nevertheless of importance as a contribution to existing knowledge.

**TECHNICAL MEMORANDUMS:** Information receiving limited distribution because of preliminary data, security classification, or other reasons.

**CONTRACTOR REPORTS:** Scientific and technical information generated under a NASA contract or grant and considered an important contribution to existing knowledge.

**TECHNICAL TRANSLATIONS:** Information published in a foreign language considered to merit NASA distribution in English.

**SPECIAL PUBLICATIONS:** Information derived from or of value to NASA activities. Publications include conference proceedings, monographs, data compilations, handbooks, sourcebooks, and special bibliographies.

**TECHNOLOGY UTILIZATION PUBLICATIONS:** Information on technology used by NASA that may be of particular interest in commercial and other non-aerospace applications. Publications include Tech Briefs, Technology Utilization Reports and Notes, and Technology Surveys.

*Details on the availability of these publications may be obtained from:*

SCIENTIFIC AND TECHNICAL INFORMATION DIVISION  
NATIONAL AERONAUTICS AND SPACE ADMINISTRATION  
Washington, D.C. 20546